IEEE Robotics and Automation Letters (RAL) paper presented at
2024 IEEE/RSJ International Conference on Intelligent Robots and Systems (IROS)
October 14-18, 2024. Abu Dhabi, UAE

# Multidirectional Bending Soft Pneumatic Actuator With Fishbone-Like Strain-Limiting Layer for Dexterous Manipulation

Xinyu Yang, Ningbin Zhang, Xinjia Huang, Rong Bian, Miao Feng, *Graduate Student Member, IEEE*, Xiangyang Zhu, and Guoying Gu, *Senior Member, IEEE*

***Abstract*—Soft pneumatic actuators (SPAs), due to their compliance and adaptiveness, are promising solutions for manipulation. However, most SPAs have only simple motion modes and cannot perform the compound motion required for complex manipulation. In this letter, we propose a parallel-chamber actuator capable of multidirectional compound bending, short for CBPCA, to provide compound motion. The key component of the actuator is the specially trimmed fishbone-like strain-limiting layer. By differentially limiting the strain on the CBPCA surface, the layer induces the main bending while allowing lateral bending to enable multidirectional compound bending of CBPCA. Further, the layer is designable to tune the motion and mechanical properties of CBPCA. We develop a kinematic model based on constant curvature assumptions to analyze and forecast the motion of CBPCA. Further, we characterize the manipulation-related indicators of CBPCA, including workspace, passive stiffness, and blocked force. The proposed CBPCA can achieve a wide-range kite-shaped spatial workspace with a motion range of 80.5% and 76.9% actuator length in main and lateral bending directions, respectively. To verify the manipulation capability of CBPCA, we developed two typical forms of manipulators: a four-finger gripper and a three-finger anthropomorphic hand to conduct experiments. The results show that CBPCA performs effectively in dexterous manipulation where basic motion primitives and complex manipulation in activities of daily living, such as setting workpieces and installing bulbs, are well-completed.**

***Index Terms*—Anthropomorphic Hand, constraint layer design, gripper, manipulation, multidirectional bending, soft pneumatic actuator.**

Manuscript received 12 October 2023; accepted 7 February 2024. Date of publication 23 February 2024; date of current version 12 March 2024. This letter was recommended for publication by Associate Editor C. M. Nunez and Editor Y.-L. Park upon evaluation of the reviewers' comments. This work was in part supported by the National Natural Science Foundation of China under Grant 52025057 and Grant 52305029, in part by the National Natural Science Foundation of Shanghai under Grant 22511101700, in part by the State Key Laboratory of Mechanical System and Vibration under Grant MSVZD202301, in part by China Postdoctoral Innovation Talents Support Program under Grant BX20220204, and in part by China Postdoctoral Science Foundation under Grant 2022M722085. *(Corresponding authors: Xiangyang Zhu; Guoying Gu.)*

The authors are with Robotics Institute, School of Mechanical Engineering, Shanghai Jiao Tong University, Shanghai 200240, China, and also with the State Key Laboratory of Mechanical System and Vibration, Shanghai Jiao Tong University, Shanghai 200240, China (e-mail: xinweiyujing@sjtu.edu.cn; zhangnb@sjtu.edu.cn; huangxinjia@sjtu.edu.cn; bianrong98@sjtu.edu.cn; fengmiao@sjtu.edu.cn; mexyzhu@sjtu.edu.cn; guguoying@sjtu.edu.cn).

This letter has supplementary downloadable material available at https://doi.org/10.1109/LRA.2024.3369475, provided by the authors.

Digital Object Identifier 10.1109/LRA.2024.3369475

## I. Introduction

DUE to the adaptiveness and compliance, soft pneumatic actuators (SPAs) provide new ideas for manipulating objects in various environments [1], [2]. Compared to rigid actuators, SPAs can deform continuously and conformably in response to the interaction with the touched objects. In this sense, we can use more simple control schemes to achieve effective grasping and manipulation tasks [3], [4], [5]. However, the more complicated manipulation puts a higher demand on the diversity of motion modes of SPAs, as it determines the maximum manipulable range and the variety of manipulation behaviors, including rotating, spinning, and translating.

A series of SPAs with specific deformation modes including elongation/contraction, bending, and twisting are proposed, such as fiber-reinforced actuators [6], [7], [8], [9], pneumatic networks (PneuNets) actuators [10], [11], bellow actuators [12], [13], [14], [15], and pouch actuators [16], [17], and they are further integrated into grippers and manipulators to execute grasp or manipulation tasks. However, the single motion mode by these actuators is insufficient for achieving complex tasks in different working scenarios, limiting their application in manipulation.

During the past decades, various SPA designs have been proposed to improve the motion range and diversity for complex manipulation. Researchers have tried to introduce the series arrangement of planar bending chambers in one actuator to enhance the mobility of the actuator [18], [19], [20], [21], [22], [23]. In this kind of design, the in-plane workspace can be greatly increased. For instance, Brock's group proposes soft fingers with two serial bending chambers to enlarge the in-plane workspace [18], [19], [22]. Despite the enlargement of the in-plane workspace by the series arrangement, the active motions in spatial coordinate systems (the spatial workspace), such as spatial curves and surfaces, which are crucial for spatial manipulation, can hardly be achieved.

In tackling this challenge, parallel chamber designs are proposed to provide spatial workspace. By arranging air chambers parallelly in one soft actuator, the actuator is capable of spatial motion with different inputs [23], [24], [25], [26], [27], [28], [29], [30], [31]. Kalisky et al. propose an actuator composed of three parallel bellow chambers to enable complex 3D movements [32]. Wood's group proposes a bellow actuator with two parallel chambers, which is capable of multilateral bending.

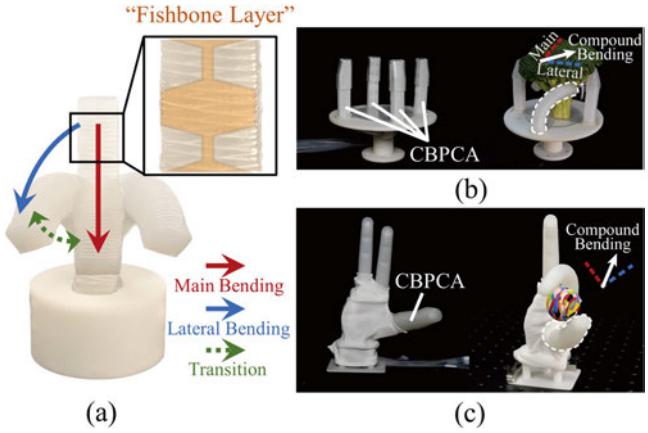


Fig. 1. Multidirectional compound bending parallel-chamber actuator (CBPCA) with fishbone-like constraint layer and its applications. (a) The main multidirectional bending modes of CBPCA induced by the constraint layer. (b) A four-finger gripper composed of four CBPCAs performing rotation manipulation by compound bending. (c) A three-finger anthropomorphic hand with a CBPCA thumb and two auxiliary serial-chamber fingers and its application in in-hand rotation. The compound bends are shown in the figures, and the colored dash lines denote the corresponding bending direction.

They further develop dexterous four-finger hands for in-hand manipulation [25], [26], [27].

In addition to efforts made in series and parallel chamber arrangement design, scientists are also committed to specially designing the shape and layout of air chambers and constraint layers to enhance the diversity of the motion modes [33], [34], [35], [36], [37]. With these special designs, a series of multi-mode SPAs with elongation, twisting, bending, and helix motions are proposed. For instance, Zou et al. propose a kind of SPA with multiple 3D motion modes by combining the chambers in specific arrangements [33]. Belding et al. propose a kind of semisoft pneumatic actuator with different slits on the external constraint shell, which incur bending, twisting, and other compound motions [34]. Kim et al. propose a unidirectional stretchable constraint layer to change the motion modes freely [35]. Baines et al. report that, by designing the layout of the strain-limiting layer, desired 3D shapes and motion can be attained by cylindrical chambers [38]. Despite the dexterous and multiple motion modes, the mechanical performance of these actuators, such as output force and stiffness, is insufficient due to the excessive softness of the chosen chamber structure, such as balloons, limiting their applications in real-world object manipulation tasks.

In this letter, we propose a parallel-chamber fiber-reinforced actuator called CBPCA (Compound Bending Parallel Chamber Actuator), capable of wide-range multidirectional compound bending for dexterous manipulation. The key component of CBPCA is a specially tailored fishbone-like strain-limiting layer (Fig. 1(a)). Combined with the parallel chambers, the layer can induce main bending and lateral bending of the actuator by differentially limiting the strain on the actuator surface. Therefore, multiple motion modes and a large workspace of compound bending are attained with two inputs, making it suitable for being integrated into different kinds of manipulators to fulfill complex manipulation tasks. We validate the manipulation functionality of CBPCA by applying it to two typical manipulators: a four-finger gripper and a three-finger anthropomorphic hand. Experiments are conducted to verify the effectiveness of the two hands, as Fig. 1(b), (c) show.

The main contributions of this letter are as follows. i) We propose the CBPCA with an easy-to-fabricate structure that is capable of wide-range multidirectional bending to provide the 3D motion crucial for spatial manipulation tasks. ii) We propose the method of intentionally trimming the constraint layer to induce certain motion forms, thereby augmenting the manipulation capabilities of soft actuators with simple structures, and this constraint layer is designable to tune the motion and mechanical properties of CBPCA by changing the design parameters. iii) We integrate CBPCA into two typical forms of manipulators: a four-finger gripper and a three-finger anthropomorphic hand. Further, we verify their manipulation capability in various tasks.

## II. Design and Fabrication of CBPCA

### A. Design

Fig. 2 shows the schematic structure and working principle of the multidirectional compound bending actuators. A CBPCA is composed of a fishbone-like constraint layer, a two-parallel silicone chamber, an air plug, and a reinforced fiber.

The key functional component of the actuator is the fishbone-like constraint layer including the spine part and rib part, and it is attached to the front surface of CBPCA, as shown in Fig. 2(a). As the silicone rubber attached to the constraint layer is considered non-stretchable, the spine part of the strain-limiting layer acts as an elongation restriction of the front surface which will cause main bending of the actuator when it's inflated. The rib part enables inconsistent elongation on both sides of the front surface, leading to lateral bending.

As shown in Fig. 2(b), when pressurized equally in both chambers, the elongations of the uncovered rubber on both sides are equal, meanwhile, the spine part of the layer constrains the axial elongation on the central part of the front surface, causing main bending. When pressurized differently, the uncovered rubber area under higher pressure will elongate more, leading to a lateral bending component in addition to the main bending. As a result, a multidirectional compound bending is achieved under different pressure inputs. We design the rib incisions with the trapezoidal structure to facilitate the lateral bending, as shown in Fig. 2(c). The maximum strain on the front surface is $\varepsilon_{\max} = \frac{\Delta l}{l_{silicone}} = \frac{l_1 - l_0}{l_{silicone}}$. Under the same actuator pose, we can see that the $\Delta l$ is equal, while the $l_{silicone}$ is larger because of the inclination angle, causing a smaller strain. The two-chamber actuator is adopted to provide essential driving degrees to realize the compound motion. The design parameters of CBPCA are tunable to adjust its motion and mechanical properties and the current parameters are selected as an effective illustrative example. The spine width is chosen to be the wall thickness between chambers to ensure mechanical properties and avoid affecting the free motion of the chambers. Further discussions on the effects of rib spacing and inclination angle on the CBPCA are presented in Section IV.

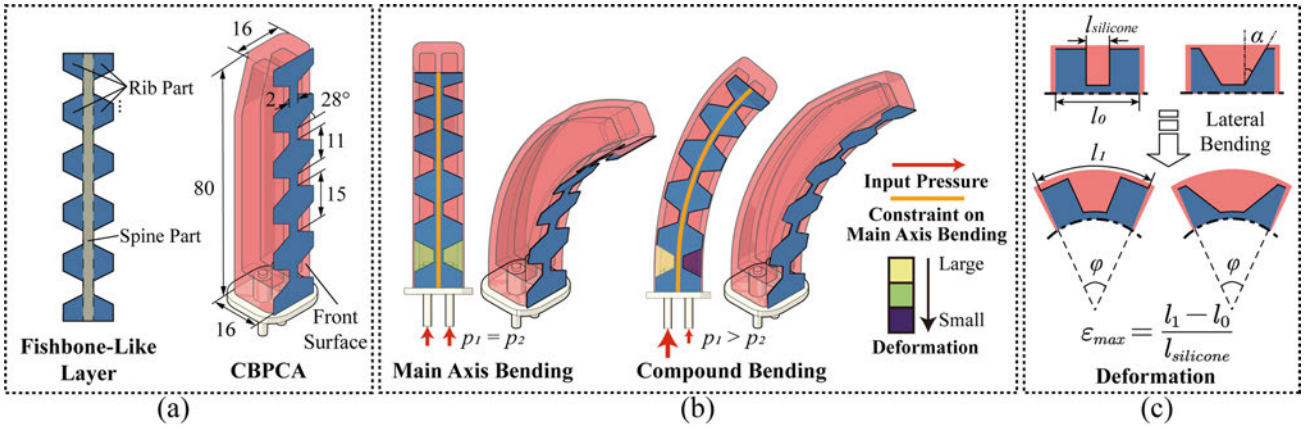


Fig. 2. Working principle of CBPCA. (a) The main structure of the fishbone-like layer and CBPCA. There are two parts in the layer: the spine part and the rib part. The design parameters are shown in this figure (unit: mm). (b) Working principle of the main multidirectional bending modes. When CBPCA is inflated, the spine part will lead to the main bending component by elongation restriction. The rib part can allow inconsistent deformation on the sides of CBPCA to induce lateral bending. The winding is omitted to make the deformation clearer, and the deformation color blocks are shown only at the bottom as an example. (c) Illustration of how the inclination angle of ribs contributes to lateral bending by bringing down the maximum strain on the front surface. Here, we selected corresponding areas on half of the front surface with varying rib angles to illustrate the deformation under identical lateral bending conditions.

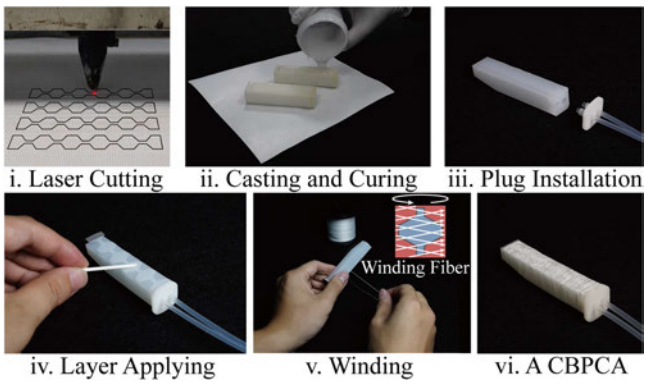


Fig. 3. Fabrication process of CBPCA.

Overall, due to the design and application of the fishbone-like constraint layer, the actuator can achieve large-range multidirectional compound bending motion.

### B. Fabrication

Fig. 3 illustrates the fabrication process of a CBPCA.

i) Use the laser cutter (VLS 3.50, Universal Laser Systems) to trim the constraint layer into the designated shape.
ii) Print the molds of the two-parallel-chamber actuator using a 3D printer (Lite 450HD, UnionTech). The two components of silicone (Dragon Skin 30, Smooth-on) are mixed thoroughly with a ratio of 1:1 and poured into the mold. Wait until the silicone is cured to get the two-chamber actuator.
iii) Install and glue (Sil-Poxy, Smooth-on) the air plug to the actuator which connects air tubes to the silicone chambers.
iv) Apply the surface treatment agent (770, Valigoo) evenly on the surface to make it more attachable. Then use quick-drying glue (502, Valigoo) to attach the fishbone layer (White Window Gauze, MuXu SiWang, with a Young's modulus of 2 GPa) to the actuator surface.
v) Wind the fiber (BRAIDED 4, YunShangPiao) evenly on the air chambers to get a CBPCA. The winding fiber is parallel in surfaces except for the front surface, where it crosses with itself in an "X" shape, as shown in the Fig. 3. The winding interval is 1mm.
vi) The actuator is re-casted with low-modulus silicone (Ecoflex 0030, Smooth-on) to obtain the outer protective/decorative silicone layer.

## III. Modeling of CBPCA

Modeling of CBPCA is conducted to further illustrate the principle of multidirectional compound motion and facilitate control in subsequent applications. The proposed model establishes the relationship between input pressures and the corresponding actuator pose, through an intermediate variable of chamber lengths. The kinematic part of the model based on the constant curvature assumptions reveals the relationship between chamber lengths and the resulting pose. To complete the model, the relationship between input pressures and chamber lengths is experimentally obtained.

To accurately depict the actuator pose and illustrate the motion mechanism of the actuator, considering the physical structure, the constant curvature modeling method is introduced [32], [39]. The typical constant curvature model is shown in Fig. 4(a). A platform is actuated by three parallel actuators ($l_1$, $l_2$, and $l_3$). By controlling their lengths, the desired platform pose can be attained. Here, the centerline $l$ connects the centroids of the two triangles where the endpoint is located. The coordinate frames are shown in Fig. 4(a) as well. To completely define the pose of the whole actuator, three parameters are introduced: $\kappa$, $\Phi$, and $l$, representing the centerline curvature, the deviation angle between the bending plane and the $xoz$ plane, and the centerline length.

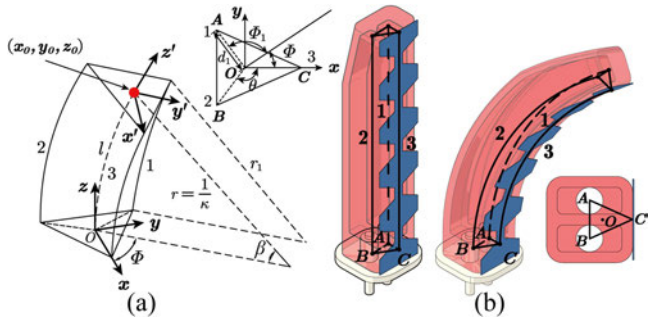


Fig. 4. Constant curvature modeling principle and corresponding illustration on the CBPCA. (a) Sketch illustration of constant curvature modeling method and the section view where main parameters and coordinate frame are defined. (b) Illustration of the CBPCA and its modeling skeleton in both original and bending positions. Line 1,2 correspond to actuating chambers, and line 3 corresponds to the spine constraint layer. Its sectional view is shown as well.

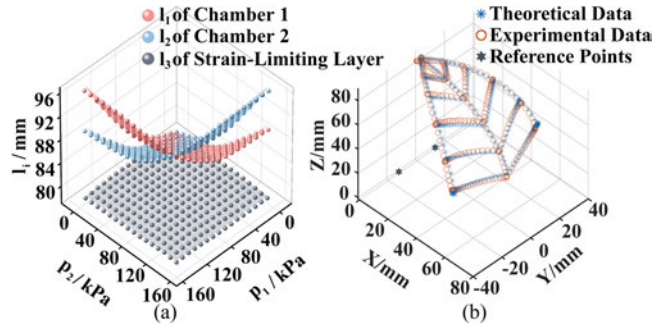


Fig. 5. Fitting and validation of the mechanical model. (a) The fitting relationship between actuating pressures and lengths of the actuators. (b) Results of the trajectory tracking experiment.

Due to the symmetry and periodicity of the fishbone-like constraint layer, the whole actuator will deform into an arc when inflated. Here, an extended constant curvature model is used to describe the motion of CBPCA. From Fig. 4, we can see the corresponding relationship between the physical structure of CBPCA and the schematic model. The spine part of the constraint layer is considered to be an air chamber with an unchangeable length. The centerline of the CBPCA is located in the centroid of the isosceles triangle where AC = BC. The cross-sections are shown in Fig. 4 as well.

Then, $\kappa$, $\Phi$, and $l$ can be obtained from the given actuator lengths as follows. All the lines are regarded to bend to the same angle $\beta$, therefore we can deduce that the radius curvature $r_i = r - d_i \cos\Phi_i$. Multiplying it by the arc angle $\beta$, we deduce that $l = l_i + \beta d_i \cos\Phi_i$. By summing the equations for all the lines, considering the characteristics of the triangle that $\sum d_i \cos\Phi_i = 0$, we can obtain that

$$l = \frac{l_1 + l_2 + l_3}{3} \tag{1}$$

Also, we can get $l = l_1 + \beta d_1 \cos\Phi_1 = l_2 + \beta d_2 \cos\Phi_2$. By considering the relationship between $\Phi_i$, $\theta$, and $\Phi$, one can get

$$\Phi = \tan^{-1}\left(\frac{3\,(l_1 - l_2)}{l_1 + l_2 - 2l_3}\cot\theta\right) \tag{2}$$

Then, applying $\beta = \kappa l$ to $l = l_i + \beta d_i \cos\Phi_i$, we can obtain

$$\kappa = \frac{l - l_i}{l d_i \cos\Phi_i} = \frac{\sqrt{9\,(l_1 - l_2)^2 \cot^2\theta + (l_1 + l_2 - 2l_3)^2}}{d_3\,(l_1 + l_2 + l_3)} \tag{3}$$

where $d_3$ and $\theta$ are parameters of the bottom isosceles triangle, as shown in Fig. 4(a).

Then, the transform matrix $T_w$ between the end pose and the global frame can be expressed by $\kappa$, $\Phi$, and $l$.

$$T_w = \begin{bmatrix} c_\Phi^2\,(c_{\kappa l} - 1) + 1 & s_\Phi c_\Phi\,(c_{\kappa l} - 1) & c_\Phi s_{\kappa l} & \frac{c_\Phi(1 - c_{\kappa l})}{\kappa} \\ s_\Phi c_\Phi\,(c_{\kappa l} - 1) & c_\Phi^2\,(1 - c_{\kappa l}) + c_{\kappa l} & s_\Phi s_{\kappa l} & \frac{s_\Phi(1 - c_{\kappa l})}{\kappa} \\ -c_\Phi s_{\kappa l} & -s_\Phi s_{\kappa l} & c_{\kappa l} & \frac{s_{\kappa l}}{\kappa} \\ 0 & 0 & 0 & 1 \end{bmatrix} \tag{4}$$

where $c_\Phi$, $c_{\kappa l}$, $s_\Phi$, $s_{\kappa l}$ are $\cos\Phi$, $\cos\kappa l$, $\sin\Phi$, $\sin\kappa l$ respectively. The end pose can then be obtained from $T_w$. Here, we derive the kinematic model of CBPCA and can obtain its end pose when the actuator lengths are given.

To complete the model, the relationship between input pressures and the air chamber lengths is experimentally measured and fitted. The experiment and fitting process are as follows. First, the CBPCA is actuated by a pressure grid ranging from 0 kPa to 150 kPa by steps of 10 kPa. The endpoint coordinates are measured by the optical tracking system. Then, the transform matrix $T_w$ is used to solve the air chamber lengths in corresponding pressures inversely. The corresponding relationship obtained from the experiment is shown in Fig. 5(a). Cubic surface fitting (Origin 2022, OriginLab) is used to fit the relationships between chamber lengths and pressures to trade off the accuracy (minimizing residual) and the complexity of this model. Considering the constraint layer is non-stretchable, constant plane fitting (Origin 2022, OriginLab) is used to fit the layer length. The fitting results are shown in Fig. 5(a) as well.

The results show that the two chambers are highly consistent in performance. The two fitting surfaces are approximately symmetric to the plane $p_1 = p_2$, indicating the properties of the two chambers are fairly similar. The standard error of the $l_3$ fitting is fairly small. This implies the fundamental assumption that the non-stretchable layer acts as a constant-length actuator is largely accurate.

To verify the whole model, pressure serials corresponding to a leaf-like trajectory are applied to the actuator. Meanwhile, the endpoint positions are measured and recorded. A comparison of theoretical data generated by the model and experimental data is shown in Fig. 5(b). From the results, the mechanical model is fairly effective among the spatial workspace of CBPCA with a maximum error ratio of 8.4% along the z-axis, which is the quotient of the maximum error and the maximum motion range. Error ratios along the x-axis and y-axis are 4.97% and 3.85%, respectively.

## IV. Characterization of CBPCA

CBPCA is designed to serve as the basic component of different kinds of manipulators. Therefore, the manipulation-related

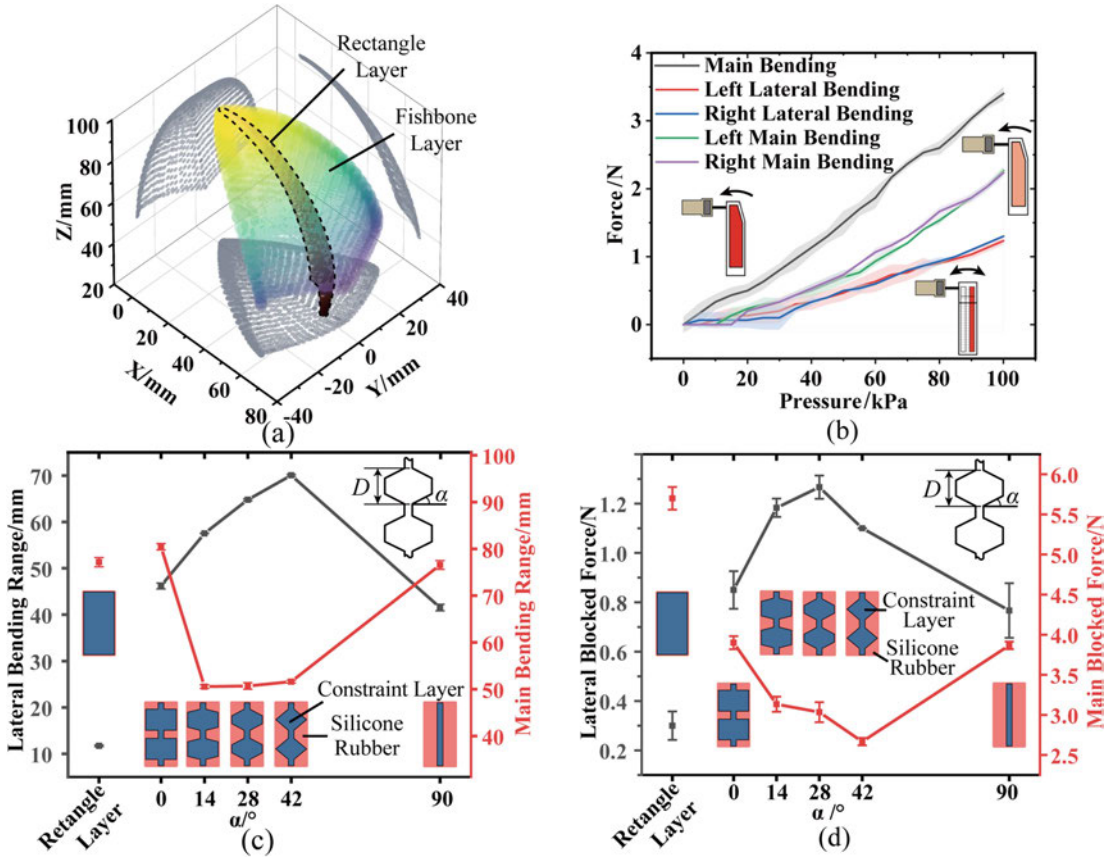


Fig. 6. Characterization of CBPCA. (a) Measured workspace of the CBPCA. The kite-shaped workspace illustrates the capacity of CBPCA to fulfill multidirectional compound bending. The workspace of the actuator with the rectangular constraint layer is also measured for comparison to show the utility of the fishbone layer. (b) Measured blocked force with different actuating modes of the CBPCA. (c) The relationship between the rib inclination angle and the multidirectional bending capacities. The maximum angle is selected to be 42° to ensure the ribs can cover the front surface. The rectangle layer and layer with only the spine part are measured for comparison. (d) The relationship between the rib inclination angle and the output forces.

capability are of great concern. Herein, to verify the mechanical performance of CBPCA, workspace, passive stiffness, and blocked force are measured and analyzed, which are closely related to spatial manipulation range, disturbance resisting ability, and manipulation robustness.

TABLE I
RELATIONSHIP BETWEEN RIB NUMBERS AND MOTION CAPACITY

| Rib Numbers N | Lateral Bending Range | Main Bending Range |
|---|---|---|
| **3** | 73.74 mm | 52.98 mm |
| **4** | 68.37 mm | 55.38 mm |
| **5** | 63.25 mm | 60.99 mm |
| **6** | 61.11 mm | 62.81 mm |

### *A. Workspace*

The workspace of CBPCA is significant as it determines the types of objects that can be manipulated and the corresponding achievable range of manipulation. In order to evaluate the workspace of the proposed CBPCA, we apply sweeps of actuation pressures (0 kPa to 150 kPa) to the two air chambers and use the optical tracking system (Motive, OptiTrack) to measure the coordinates of the actuator endpoint. The workspace of a two-chamber actuator with the untreated rectangle constraint layer is also measured for comparison. The 3D measurement result is shown in Fig. 6(a). It can be seen from the comparison that the introduction of the specially trimmed constraint layer can greatly facilitate lateral bending and enable a wider range of multidirectional bending, which will boost the manipulation ability of CBPCA, with the normalized lateral motion increased by 550% compared to the rectangle constraint.

The shape of the CBPCA workspace resembles an inverted kite. It has a range of about 63 mm in the main bending direction (X-axis), ±30 mm in the lateral direction (Y-axis), and 48 mm in the Z-axis with the whole length only 78 mm. The working ranges normalized by the actuator length are about 0.805, 0.769, and 0.615 on the XYZ-axis respectively. From the results, the motion ranges are comparable to the actuator length and the objects to be manipulated, sufficient to enable wide-range manipulation.

We further investigated the influence of design parameters on the workspace, specifically the rib spacing and inclination angle. CBPCAs with different constraint layer design parameters are fabricated and tested using the aforementioned testing methods. As shown in Table I, with the rib spacing increasing (the rib number decreasing), the lateral motion is enhanced slightly

while the bending is reduced slightly. The more influential parameter is the inclination angle. With the angle increasing, the lateral motion capacity is greatly enhanced, as shown in Fig. 6(c). The maximum angle is of 42° at which the fishbone shape can effectively constrain the rubber due to the geometric constraint. We can see from Fig. 6(c) that the introduction of the fishbone layer greatly enhances the lateral bending range.

The actuation time is considered to reflect the dynamic characteristics. We test the time the CBPCA takes to enclose and recover in both directions at working pressures (150 kPa). The time CBPCA takes to bend and recover in the main bending direction is 511±17 ms and 689±16 ms, while it is 517±32 ms and 756±46 ms in the lateral bending direction, respectively. The results show that CBPCA is fast enough to handle the manipulation tasks mentioned in our work.

### B. Passive Stiffness

To evaluate the mechanical performance of CBPCA, passive stiffness is studied first, which refers to the stiffness at uninflated state. It primarily depends on the inherent characteristics of CBPCA and reflects the actuator's capacity to bear a load, transfer force, and withstand unexpected disturbances.

To measure the stiffness in both the main bending and lateral bending planes, a CBPCA is fixed to the ground, acting as a cantilever. Subsequently, a force sensor (LSB200, Futek) is used to deflect the finger by 10 mm in the corresponding bending plane, simultaneously measuring the deformation and output force. The average stiffness can be obtained from the slope of the force-displacement curve. The experiment is carried out three times. From the experiments, the main bending and the lateral stiffnesses are 46.17±1.72 N/m and 26.33±1.51 N/m, respectively, which is comparable to the state of the art [18], [25], potentially ensuring a stable grasp during manipulation against disturbance.

### C. Blocked Force

Another important metric to evaluate an actuator's mechanical performance is the blocked force. Unlike passive stiffness, blocked force mainly reflects active performance, that is the ability to output force and interact with objects.

To measure the output force in the main and lateral bending directions, a CBPCA is fixed in a semi-enclosed fixture with only one side open. A force sensor is placed in front of the open side and its probe is in alignment with the actuator tip. When measuring the blocked force, the corresponding actuator surface is set in opposition with the probe.

The experiment is carried out with different chambers inflated to obtain full information about the output force in different directions, and the results are shown in Fig. 6(b). Here, the pressure range is selected to be 0 kPa to 100 kPa. From the results, we can see the consistency of the two chambers is relatively high. The main bending and lateral blocked force when only one chamber is inflated are about 2.25 N and 1.27 N respectively. The maximum blocked force under the actuation of two chambers is about 3.40 N. The output force is sufficient for stable grasp and robust manipulation of daily objects, as shown in [9], [18], [25], [40], which is also validated in the following applications. As shown in Fig. 6(d), with the increase of the inclination angle, the lateral force is enhanced while the bending force is reduced except for 42°, where the area of the layer is the smallest. Overall, the tendency is in high correspondence of the relationship between the inclination angle and motion.

## V. Application of CBPCA in Manipulators

To verify the performance of the proposed actuators in real-world manipulation tasks, two typical forms of manipulators: a four-finger gripper and a three-finger anthropomorphic hand are used as platforms to carry out various manipulation experiments to comprehensively validate the utility of CBPCA. The gripper represents application in standardized manipulation like industrial scenarios, where collaborative gaits of CBPCAs are needed. The anthropomorphic hand represents application in daily life on objects designed for human hands, where the CBPCA dominates human-like manipulation.

### A. Four-Finger Gripper

The proposed four-finger gripper is shown in Fig. 7(a). Four CBPCAs are equally spaced on a circle with a radius of 60 mm, and installed on the costumed 3D-printed fixture. Gel finger stalls (ThumbStall, Menthogel) are applied to finger tips to increase friction coefficient.

In order to showcase the utility and versatility of the compound bending actuators and the gripper, continuous rotation and translation gait are proposed and adopted to manipulate various objects, as shown in Fig. 7(c) and (d). Cylinders, cubes of different sizes, and some daily objects are chosen to be operated by the gripper to show the generality and robustness of the control scheme, as Fig. 7(b) shows. To quantify the manipulation effect, the same rotation and translation gaits are executed continuously 5 times on objects, and meanwhile, the object poses are captured by the optical tracking system.

The planar workspaces of the translation and rotation gaits obtained from the experiments are shown in Fig. 7(e). We can see from the results that the rotation gait is effective among all the items. The rotation angles of small objects are larger because of larger finger defromation. The manipulation consistency of objects with higher axial symmetry is better, reflected in lower standard deviation, while the rotation gait is also effective for irregularly shaped objects such as cubes and broccoli. Translation gait is also of great generality among these objects. The planar workspace is slightly smaller for large items because of the external boundary formed by fingers. For irregularly shaped objects, the translation gait is also effective. Overall, the two gaits are fairly effective for the gripper. Furthermore, the model developed in Section III can be utilized to adjust the pressure sequence accordingly to enhance the manipulation capability for various objects.

Further, functional tasks such as bulb installation, bottle uncapping, and workpieces setting can be achieved, as shown in Fig. 7(f). By combining basic motion primitives, complex manipulation can be achieved by a simple structure, showing the functionality of the dexterous actuator and gripper.

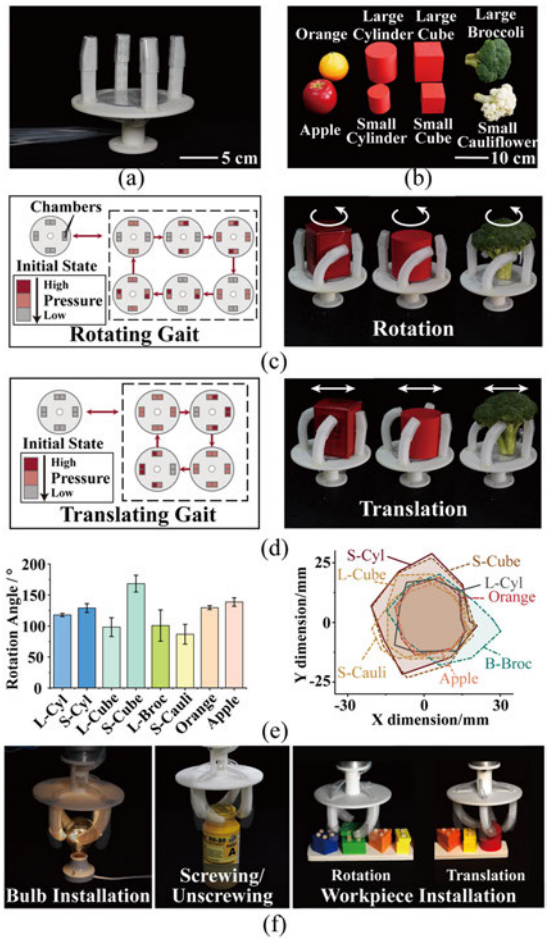


Fig. 7. Four-finger gripper and its manipulating abilities. (a) The four-finger gripper. (b) Objects to be manipulated. (c) Control scheme of rotating gait and application on objects. (d) Control scheme of translating gait and application on objects. (e) Manipulating abilities on rotation and translation of objects, which is the average rotation angle and planar motion range in one cycle, respectively. (f) Functional manipulation tasks. The hand can install bulbs, screw/unscrew bottle caps and install workpieces by the finger gaits.

### *B. Three-Finger Anthropomorphic Hand*

As Fig. 8(a) shows, the anthropomorphic hand comprises three fingers. The thumb takes the form of CBPCA, and the other two auxiliary fingers (index and middle) are ordinary two-serial-chamber actuators. These three fingers are selected to retain the main structure and functionality of human hand. The thumb here undertakes the manipulation tasks due to its compound bending motion, while the other two fingers play a supporting role by providing grasping forces or helping adjust objects' poses.

In human manipulation, the common workspace is an important concept representing the manipulating capacity [20]. It refers to the common area of different fingers' workspace. A larger common workspace implies having the ability to contact an object in more different poses and move it over a larger range, which forms the foundation for dexterous manipulation. Therefore, it's important to characterize the common workspace of the thumb and other fingers. The thumb's workspace is determined by driving the servo-actuated carpometacarpal (CMC) joint placed at the finger base to different angles and applying the pressure girds.

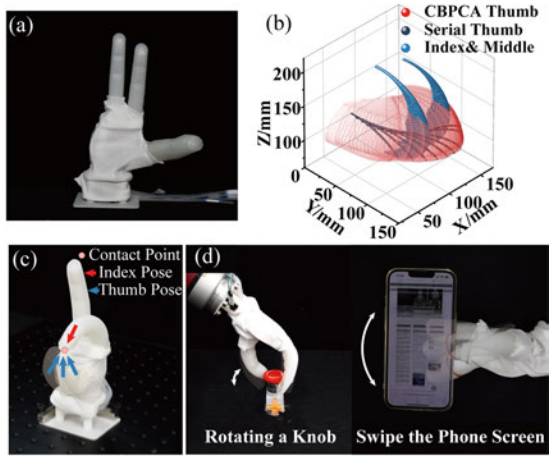


Fig. 8. Three-finger anthropomorphic hand and its manipulating abilities. The hand is composed of a thumb (CBPCA), index, and middle finger (simple bending actuators). (a) The three-finger anthropomorphic hand. (b) The common workspace of the CBPCA thumb and the other fingers. A two-serial-chamber thumb is also used for comparison. (c) Thumb opposition experiment with various thumb positions. (d) Finishing manipulation tasks.

The workspaces of the CBPCA thumb and the other fingers are shown in Fig. 8(b). For comparison, a two-serial-chamber thumb with the same size is adopted and its workspace is measured as well. It can be clearly seen from Fig. 8(b) that compared to the 2D curve workspace of the serial-chamber thumb, the workspace of the CBPCA thumb is a quite larger spatial surface. And by applying different CMC angles, the CBPCA thumb can sweep a wide range of spatial workspace, providing larger common workspace with the other two fingers. This will further enable more complicated continuous translation and rotation and can provide an extrodinary advantage in spatial manipulation compared to the serial thumb with only in-plane motion.

To demonstrate the dexterity of the anthropomorphic hand, various experiments are conducted including multi-pose thumb oppositon and functional tasks execution. The thumb opposition experiment is to actuate the thumb by the CMC joint and pressure inputs to touch the same point (the index finger tip) in different gestures, as shown in Fig. 8(c). The opposition experiment illustrates that the hand has the potential to manipulate objects in various poses, which is consistent to the analysis of the common workspace in Fig. 8(b). By appropriately actuating the thumb and auxiliary fingers, translation and rotation can be also achieved. It's worth noting that the rotation around the palm-vertical axis can be achieved by only actuating the thumb finger without the assistance of the CMC joint and any other fingers. By utilizing these motion primitives on objects, various tasks can be achieved by the hand, as Fig. 8(d) shows. The rotation primitive can be used to rotate a knob and install bulbs, and the hand can swipe the phone screen with only the thumb actuated. CMC joint is fixed in these experiments.

Overall, by utilizing CBPCA as the thumb, a larger common workspace can be achieved, enabling multi-pose thumb opposition, basic motion primitives, and versatile manipulation.

## VI. Conclusion

Focusing on improving the diversity of actuator motion to achieve dexterous manipulation, in this letter, we proposed a parallel-chamber actuator capable of wide-range multidirectional bending, featuring a fishbone-like constraint layer. The introduced layer can induce versatile bending motions, thereby augmenting the manipulation capacity. Furthermore, it's designable to tune the motion and mechanical properties of CBPCA by changing design parameters. Compared to the actuator with a rectangle constraint layer, the CBPCA can achieve a wider-range kite-like workspace, with a motion range of 80.5% and 76.9% actuator length in main and lateral bending directions, respectively. The mechanical performance of CBPCA is also characterized. The overall characterization demonstrates that our proposed CBPCA guarantees a wide motion range, robust grasp, and powerful manipulation. To further evaluate CBPCA's capability in real-world manipulation, it's integrated into two typical forms of manipulators: a gripper and a anthropomorphic hand. Effective motion primitives and versatile manipulation can be attained by the two platforms, showing the functionality of the proposed CBPCA.

The method of specially trimming the constraint layer to get the expected motion can be further extended to general soft actuators. In future work, we will further explore the relationship and try to propose the inverse design method. We will also try to propose more efficient finger gaits to achieve more complicated manipulation in various environments.

## References


[1] A. Billard and D. Kragic, "Trends and challenges in robot manipulation," *Science*, vol. 364, no. 6446, 2019, Art. no. eaat8414.

[2] M. T. Mason, "Toward robotic manipulation," *Annu. Rev. Control, Robot., Auton. Syst.*, vol. 1, no. 1, pp. 1–28, 2018.

[3] D. Rus and M. T. Tolley, "Design, fabrication and control of soft robots," *Nature*, vol. 521, no. 7553, pp. 467–475, May 2015.

[4] N. Hogan, "Contact and physical interaction," *Annu. Rev. Control, Robot., Auton. Syst.*, vol. 5, no. 1, pp. 179–203, May 2022.

[5] J. K. A. Langowski, P. Sharma, and A. L. Shoushtari, "In the soft grip of nature," *Sci. Robot.*, vol. 5, no. 49, Dec. 2020, Art. no. eabd9120.

[6] F. Connolly, C. J. Walsh, and K. Bertoldi, "Automatic design of fiber-reinforced soft actuators for trajectory matching," *Proc. Nat. Acad. Sci. USA*, vol. 114, no. 1, pp. 51–56, Jan. 2017.

[7] G. Singh and G. Krishnan, "Designing fiber-reinforced soft actuators for planar curvilinear shape matching," *Soft Robot.*, vol. 7, no. 1, pp. 109–121, Feb. 2020.

[8] H. Zhao et al., "Optoelectronically innervated soft prosthetic hand via stretchable optical waveguides," *Sci. Robot.*, vol. 1, no. 1, 2016, Art. no. eaai7529.

[9] G. Gu et al., "A soft neuroprosthetic hand providing simultaneous myoelectric control and tactile feedback," *Nature Biomed. Eng.*, vol. 7, no. 4, pp. 589–598, 2023.

[10] B. Mosadegh et al., "Pneumatic networks for soft robotics that actuate rapidly," *Adv. Funct. Mater.*, vol. 24, no. 15, pp. 2163–2170, Apr. 2014.

[11] G. Gu et al., "Analytical modeling and design of generalized pneu-net soft actuators with three-dimensional deformations," *Soft Robot.*, vol. 8, no. 4, pp. 462–477, Aug. 2021.

[12] R. Balak and Y. C. Mazumdar, "Multi-modal pneumatic actuator for twisting, extension, and bending," in *Proc. IEEE/RSJ Int. Conf. Intell. Robots Syst.*, 2020, pp. 8673–8679.

[13] D. Drotman, M. Ishida, S. Jadhav, and M. T. Tolley, "Application-driven design of soft, 3-D printed, pneumatic actuators with bellows," *IEEE/ASME Trans. Mechatronics*, vol. 24, no. 1, pp. 78–87, Feb. 2019.

[14] X. Dong, C. Tang, S. Jiang, Q. Shao, and H. Zhao, "Increasing the payload and terrain adaptivity of an untethered crawling robot via soft-rigid coupled linear actuators," *IEEE Robot. Automat. Lett.*, vol. 6, no. 2, pp. 2405–2412, Apr. 2021.

[15] N. Zhang et al., "3D printed, modularized rigid-flexible integrated soft finger actuators for anthropomorphic hands," *Sensors Actuators A, Phys.*, vol. 312, 2020, Art. no. 112090.

[16] R. Niiyama, D. Rus, and S. Kim, "Pouch motors: Printable/inflatable soft actuators for robotics," in *Proc. IEEE Int. Conf. Robot. Automat.*, 2014, pp. 6332–6337.

[17] R. Niiyama et al., "Pouch motors: Printable soft actuators integrated with computational design," *Soft Robot.*, vol. 2, no. 2, pp. 59–70, 2015.

[18] S. Puhlmann, J. Harris, and O. Brock, "RBO hand 3: A platform for soft dexterous manipulation," *IEEE Trans. Robot.*, vol. 38, no. 6, pp. 3434–3449, Dec. 2022.

[19] A. Sieler and O. Brock, "Dexterous soft hands linearize feedback-control for in-hand manipulation,", in *Proc. IEEE/RSJ Int. Conf. Intell. Robots Syst.*, pp. 8757–8764, 2023.

[20] J. Zhou et al., "A soft-robotic approach to anthropomorphic robotic hand dexterity," *IEEE Access*, vol. 7, pp. 101483–101495, 2019.

[21] C. B. Teeple et al., "Multi-segment soft robotic fingers enable robust precision grasping," *Int. J. Robot. Res.*, vol. 39, no. 14, pp. 1647–1667, Dec. 2020.

[22] A. Bhatt et al., "Surprisingly robust in-hand manipulation: An empirical study," in *Proc. Conf. Robot. Sci. Syst. XVII*, 2021, doi: 10.15607/RSS.2021.XVII.089.

[23] R. Zhen et al., "Modular bioinspired hand with multijoint rigid-soft finger possessing proprioception," *Soft Robot.*, vol. 10, no. 2, pp. 380–394, 2023.

[24] Z. Gong et al., "A soft manipulator for efficient delicate grasping in shallow water: Modeling, control, and real-world experiments," *Int. J. Robot. Res.*, vol. 40, no. 1, pp. 449–469, 2021.

[25] S. Abondance, C. B. Teeple, and R. J. Wood, "A dexterous soft robotic hand for delicate in-hand manipulation," *IEEE Robot. Automat. Lett.*, vol. 5, no. 4, pp. 5502–5509, Oct. 2020.

[26] C. B. Teeple, R. C. S. Louis, M. A. Graule, and R. J. Wood, "The role of digit arrangement in soft robotic in-hand manipulation," in *Proc. IEEE/RSJ Int. Conf. Intell. Robots Syst.*, 2021, pp. 7201–7208.

[27] C. B. Teeple, G. R. Kim, M. A. Graule, and R. J. Wood, "An active palm enhances dexterity of soft robotic in-hand manipulation," in *Proc. IEEE Int. Conf. Robot. Automat.*, 2021, pp. 11790–11796.

[28] Y. Zhang et al., "Human-powered master controllers for reconfigurable fluidic soft robots," *Soft Robot.*, vol. 10, pp. 1126–1136, 2023.

[29] R. L. Truby, C. D. Santina, and D. Rus, "Distributed proprioception of 3D configuration in soft, sensorized robots via deep learning," *IEEE Robot. Automat. Lett.*, vol. 5, no. 2, pp. 3299–3306, Apr. 2020.

[30] T. Kalisky et al., "Differential pressure control of 3D printed soft fluidic actuators," in *Proc. IEEE/RSJ Int. Conf. Intell. Robots Syst.*, 2017, pp. 6207–6213.

[31] B. Shih et al., "Custom soft robotic gripper sensor skins for haptic object visualization," in *Proc. IEEE/RSJ Int. Conf. Intell. Robots Syst.*, 2017, pp. 494–501.

[32] R. K. Katzschmann, C. D. Santina, Y. Toshimitsu, A. Bicchi, and D. Rus, "Dynamic motion control of multi-segment soft robots using piecewise constant curvature matched with an augmented rigid body model," in *Proc. 2nd IEEE Int. Conf. Soft Robot.*, 2019, pp. 454–461.

[33] J. Zou et al., "Muscle-fiber array inspired, multiple-mode, pneumatic artificial muscles through planar design and one-step rolling fabrication," *Nat. Sci. Rev.*, vol. 8, no. 10, Nov. 2021, Art. no. nwab048.

[34] L. Belding et al., "Slit tubes for semisoft pneumatic actuators," *Adv. Mater.*, vol. 30, no. 9, Mar. 2018, Art. no. 1704446.

[35] S. Y. Kim et al., "Reconfigurable soft body trajectories using unidirectionally stretchable composite laminae," *Nature Commun.*, vol. 10, no. 1, Dec. 2019, Art. no. 3464.

[36] P. Jiang et al., "A novel scaffold-reinforced actuator with tunable attitude ability for grasping," *IEEE Trans. Robot.*, vol. 39, no. 2, pp. 1164–1177, Apr. 2023.

[37] Z. Kan et al., "Soft actuator with programmable design: Modeling, prototyping, and applications," *Soft Robot.*, vol. 9, no. 5, pp. 907–925, Oct. 2022.

[38] R. Baines et al., "Programming 3D curves with discretely constrained cylindrical inflatables," *Adv. Materials*, vol. 35, Mar. 2023, Art. no. 2300535.

[39] R. J. Webster and B. A. Jones, "Design and kinematic modeling of constant curvature continuum robots: A review," *Int. J. Robot. Res.*, vol. 29, no. 13, pp. 1661–1683, Nov. 2010.

[40] H. Wang, F. J. Abu-Dakka, T. N. Le, V. Kyrki, and H. Xu, "A novel soft robotic hand design with human-inspired soft palm: Achieving a great diversity of grasps," *IEEE Robot. Automat. Mag.*, vol. 28, no. 2, pp. 37–49, Jun. 2021.